5-7-2016

Low-Energy Impact of Human Cartilage: Predictors for Fracturing the Network of Collagen

Bilal Kaleem
University of Connecticut - Storrs, bilal.kaleem@uconn.edu

Low-Energy Impact of Human Cartilage: Predictors for Fracturing the Network of Collagen

Bilal Kaleem

B.S., University of Connecticut, 2014

A Thesis

Submitted in Partial Fulfillment of the

Requirements for the Degree of

Master of Science

At the

University of Connecticut

2016

2016

APPROVAL PAGE

Masters of Science Thesis

Low-Energy Impact of Human Cartilage: Predictors for Fracturing the Network of Collagen

Presented by

Bilal Kaleem, B.S.

Major Advisor: Dr. David Pierce

Associate Advisor: Dr. Wendy Vanden Berg-Foels

Associate Advisor: Dr. Bin Feng

Committee Member: Dr. George Lykotrafitis

University of Connecticut

2016

Dedication

To my parents, who each own half of my degree.

To my wife, who made the last year of graduate school a little more bearable.

Acknowledgment

I would like to thank Dr. David Pierce, for his guidance and encouragement throughout the pursuit of my research. The knowledge I have gained from him will be invaluable throughout my life.

I would like to thank my committee members, Dr. Bin Feng, Dr. Wendy Vanden Berg-Foels, and Dr. George Lykotrafitis for their review of this thesis.

I would like to thank my lab member, Franz Maier for his assistance in developing and executing this research. I would also like to thank Stephany Santos and Jon Kaplan for their support.

I would like to thank Andrew Cohen and Chamoussoudine Kandjrika for their support in collecting and analyzing data.

I thank the Musculoskeletal Transplant Foundation for providing us with human tissue samples.

I thank Tom Mealy and Michael Difrancesco for help in constructing the low-energy impact tester.

Contents

1 Introduction **3**

1.1 Literature Review 3

2 Methods **18**

2.1 Materials and Methods 18

2.2 Specimen Preparation 18

2.3 Low-Energy Impact Testing 19

2.4 Data Analysis 20

2.5 SHG Imaging 21

2.6 Image Analysis 22

2.7 Statistical Analysis 22

3 Results **24**

3.1 Low-Energy Impact Testing and Data Analysis 24

3.2 SHG Imaging and Image Analysis 26

3.3 Statistical Analysis 26

4 Discussion **31**

4.1 Low-Energy Impact Testing and Data Analysis 31

4.2 SHG Imaging and Image Analysis 32

4.3 Statistical Analysis 33
4.4 Limitations and Outlook 34

Abstract

We aimed to determine the minimum mechanical impact to cause microstructural damage (micro-fractures) in the network of collagen within human cartilage and hypothesized that energies well below 0.1 J or 1 mJ/mm^3 would cause such damage. We completed 108 low-energy impact tests (0.05, 0.07, 0.09 J at 0.75 or 1.0 m/s) using healthy cartilage specimens from six male donors. Before and after impact we acquired, imaging the second harmonic generation, ten images from each specimen (50 μm depth, 5 μm step size), resulting in 2160 images. We quantified both the width and depth of micro-fractures. We then correlated predictors (test parameters) impact energy/energy dissipation density, nominal stress/stress rate, and strain/strain rate to micro-fracture in the collagen network and tested for significance. In cases where predictors significantly correlated with microstructural outcomes we fitted a binary logistic regression plot with a 95% confidence interval. No specimens showed visible damage following impact. We found that impact energy/energy dissipation density and nominal stress/stress rate were significant ($p < 0.05$) predictors of micro-fractures while both strain and strain rate were not. In our test configuration, an impact energy density of 3.30 mJ/mm^3, an energy dissipation density of 1.90 mJ/mm^3, a nominal stress of 4.60 MPa, and a nominal stress rate 764 MPa/s all corresponded to a 50% probability of micro-fracture. Impact energy densities as low as 0.208 mJ/mm^3 corresponded to a 10% probability of micro-fractures in the network of collagen within human cartilage. Such changes may initiate the degenerative cascade known as post-traumatic

osteoarthritis.

1 Introduction

1.1 Literature Review

Articular cartilage provides an extremely low friction material to pad the surfaces of articulating bones. Its unique structure provides remarkable strength and durability for its role in joint stabilization. Chondrocytes embedded in a fibrous collagen matrix with fluid and proteoglycans make up articular cartilage. Because cartilage is a mechanically important tissue, the bod, chondrocytes constantly remodel it and adapts the tissue to a changing environment. However, in mature articular cartilage, there is only scarce presence of chondrocytes and the regeneration of cartilage is limited. This makes many different types of trauma dangerous for the health of cartilage and can induce a destructive path for the tissue. Once such path is the development of osteoarthritis, a disorder that is characterized with the degeneration of articular cartilage. Previous studies have researched the cause for osteoarthritis and one possible cause is traumatic impact to the tissue. Impact loading on cartilage has been shown to produce fissures on the surface and alter the collagen fiber structure throughout the tissue. This in turn, alters the tissues ability for water retention and further hampers its function as a supportive, shock-absorbing material for bone. This type of trauma directly affects the structure of cartilage and there should be a focus on quantifying this dramatic change. A quantitative understanding of this change will reveal how the function is modified.

Jeffrey et al. (1995) studied the effect of impact loads on the matrix integrity and chondrocyte viability of articular cartilage. Bovine articular cartilage from the carpo-metacarpal joint of 16 to 20 month old animals were obtained and 15 full-depth, 5 mm diameter samples were extracted. Due to difficulties in sample extraction, some cartilage samples were removed from the attached bone. A drop tower was used to apply the impact. A 100 g weight was used with drop heights of 5 cm, 10 cm, 20 cm, and 50 cm, 500 g weight with 2 cm, 5 cm, 10 cm, and 20 cm, and 1000 g weight with 2 cm, 5 cm, and 10 cm. These weights and heights were used to produce observable damage from mild to severe. An accelerometer measured the dynamics of the impactor and velocity and displacement were calculated using and one and two steps of integration respectively. From this, stress and strain were calculated. Water content was measured by weighing the samples before and after impact daily for up to 15 days maintained in culture. Chondrocyte viability was measured by digesting the collagen present using collagenase in 37oC. Then the samples were stained with trypan blue and the chondrocytes were counted with a hemocytometer. Histology was conducted by fixation in neutral buffered formaldehyde and stained with van Gieson for collagen or toluidine blue for glycosaminoglycans (GAG). Finally, SEM was conducted to review the fracture surface of the samples. The results showed that visible damage increased with impact energy. Also, there was a considerable effect on the mass of the sample following impact. Immediately after impact, the samples showed a considerable decrease in mass; there was a 60% decrease in mass for an impact of 500 g from 20 cm. Following 2 days in culture, the sample increased in mass up to a 60% increase from the unloaded mass. Chondrocyte viability was largely unaffected by the lowest testing parameters however for samples using the 500 g 2 cm test parameter, viability dropped to 40%. Finally, SEM showed fissuring on samples that were removed from the bone that was much more severe than those present on samples with the bone attached. The researchers were able to show the biochemical effects of impact trauma on cartilage, there should be

more focus on a more precise characterization of the structural changes in the tissue. Converting the observed damage to clinically accepted assessment scores would allow for a more standardized relation between impact trauma and damage progression.

Jeffrey et al. (1997) studied the biochemical effects of an impact on articular cartilage by measuring the changes in matrix components in the tissue. This study differs from the previous one because it utilizes radiolabeling to identify uptake and release of precursors to matrix components. Articular cartilage samples were extracted from bovine carpo-metacarpal joints of 16-20 month old calves. Up to 10 full-depth plugs, 5 mm in diameter, were removed from the medial surface of the metacarpal bone. They were soaked in Hams F12 culture medium mixed with either [^{3}H]leucine for protein labeling or ^{35}SO4 for GAG labeling. A drop tower utilizing gravitational potential energy was used with varying weights and drop heights: with 100 g used with 25 cm, 500 g with 2 cm, 5 cm, 10 cm, and 20 cm, and 1 kg with 2.5 cm. These ranges of weights and drop heights were used to provide a wide range of impacts that are typically experienced in accidents. The 500 g weight was used to apply different impact energies while the 100 g - 25 cm testing parameter was paired with the 1 kg 2.5 cm testing parameter to have equal impact energies but different impact velocities for comparison. The radioactive markers were measured before and after the impact to determine change in morphology. The results showed a reduction in both protein and GAG content within the samples. However, 60% of the protein content was lost while only 25% of the GAG content was lost. In addition, loss of protein content did not appear to correlate with impact energy or velocity. However, GAG content loss was found to be highly correlated to impact velocity and energy. In conclusion, more work needs to be done to fully understand how impact affects the structure of the cartilage matrix. By doing so, the progression path of osteoarthritis can be further understood.

Ewers et al. (2001) studied the effect of loading rate on the extent of matrix damage and cell death after impact loading. For this study bovine forelegs, between 18-24 months of

age, were used to extract 6.35 mm diameter plugs from the metacarpal surface of the joint. In total, 90 plugs were extracted and the subchondral bone was removed. The samples were then placed in Dulbeccos Modified Eagles Medium to minimize matrix degradation or cell death prior to the test. Thirty samples were used as a control group with no compression test and the remaining 60 were placed in two groups: high rate of loading which was about 900 MPa/s and low rate of loading which was about 40 MPa/s. The loading was applied using two plates in an unconfined environment using a servo-hydraulic machine. Peak load, time to peak load, and maximum displacement were recorded. After the test, five samples from each group were selected for a cell viability study in which 1 mm slices of the sample were made and stained with calcein and ethidium bromide homodimer. Then the samples were seen through a florescence microscope and the number of live chondrocytes (green) and dead chondrocytes (red) were counted. Finally, fissures were stained with India ink. The results showed that the peak load didnt significantly differ between the high-rate loading and low-rate loading testing. However, time to peak load, and maximum strain both showed a significant difference between the samples in the two testing protocols. Time to peak force was 43 ms for the high rate of loading while it was 1 second for the low rate. Maximum strain for the high rate group was 0.476 while for the low rate group it was 0.409. For matrix damage studies, it was found that high-rate of loading produced a higher number and severity of fissures. The cell viability study did not show any significant difference in the number of dead cells between the two loading protocols, however it was observed that most of the dead cells were near the surface for the high-rate group and dispersed through the thickness for the low-rate group. In conclusion, significant differences in the tissue behavior in terms of rate of loading were observed. An area that the researchers could have improved upon is having more testing protocols within the two selected protocols. A difference of 860 MPa/s is quite large and implementing more protocols could provide more data for further interpolation.

Jeffrey et al. (2006) conducted impact loading on human and bovine cartilage to explore different loading conditions such as impactor vs indentor and different energies of impact. Cartilage from human and bovine femoral heads were removed using a cork borer and scalpel and soaked in phosphate buffered solution(PBS). Energies of 0.12, 0.25, and 0.375 J were applied using a 500 g mass and 25 mm, 50 mm, and 75 mm drop heights. Following the impact testing, the samples were snapped into two pieces after being frozen in liquid nitrogen. One half was used for scanning electron microscopy (SEM) to assess the damage following a single impact load. The other half was used for polarizing microscopy to calculate the distribution of collagen fiber orientations. The results showed the human explants were able to withstand higher impact energies than the bovine explants. The peak stresses were 24.9 5.6 MPa and 21.7 6.5 MPa for human and bovine samples, respectively. The SEM revealed the damage caused to the cartilage, which correlated with the peak stresses sustained by the different sample species. The presence of fissures was found to be more severe in the bovine cartilage as opposed to the human, which showed little fissuring. Polarizing microscopy revealed the inner collagen fiber orientations with respect to depth. The surface and intermediate zones of the human cartilage are thicker as opposed to the bovine cartilage zones. The transition in collagen fiber orientation seemed to be much quicker in bovine cartilage. The researchers were able to relate the structure and its properties; however, more focus should be given on the effect that impact has on the tissue. A more standardized way of interpreting the damage done to the samples would help relate the results to common cases of osteoarthritis. Simply using a binary measure of fissures or no fissures is not sufficient to understand the damage effects of a traumatic impact injury.

Verteramo et al. (2007) employed a simpler impact design to measure the changes in compressive strength and response of articular cartilage to cyclic compressive loading after being subjected to a single impact. The researchers used two bovine knee joints and extracted 16 osteochondral plugs from each: 4 from posterior lateral, 4 from the posterior

medial, 4 from the anterior lateral, and 4 from the anterior medial sections of the condyle. The samples were placed in either a walking or running cyclic loading condition as defined by the researchers and the storage and loss moduli were calculated. The walking loading condition was defined as 1.5 MPa at a frequency of 1 Hz and the running loading condition as 7 Mpa at 2 Hz. The samples were then subjected to 0.49, 0.74, 1.47, or 1.96 J impact energies. The samples were placed again in the same walking or running loading conditions and the differences in storage and loss moduli were measured. The change in moduli was found to be statistically significant ($p = 0.05$) for 1.472 and 1.962 J for the level running condition and only the 1.962 J for the level walking condition. Finally, biochemical analysis was done using Toluidine blue staining to identify structural damage such as fissures on the surface of the tissue. Large fissures were found on the surface of the cartilage and in some cases; fractures reached the subchondral bone layer. Although it is important to see the physical changes caused by traumatic impact of cartilage, it must be related to the impact data for it to be clinically relevant. Simply qualitatively describing the damage done without calculating any measure provides no relationship between change in structure and change in function. Analysis showing a relationship between impact energy and size of fissure, or depth of penetration would provide data to calculate the threshold for cartilage damage.

Burgin et al. (2008) studied the effect of bone on the mechanical properties of articular cartilage during impact loading. This was achieved by progressively shortening the core of subchondral bone and also gluing the cartilage samples to substrates of different moduli under impact loading. Bovine samples, cut above the carpal joint, were used and ultimately, 108 samples of 5 mm diameter were used for cartilage-on-substrate impact testing and 10 of 9 mm diameter were used for cartilage-on-bone samples. Prior to impact testing, the cartilage samples and bone plugs were subjected to unconfined compression of up to a Cauchy stress of 0.15 MPa. A 3 mm steel plate was used to apply the compres-

sion. For impact testing, a drop tower with 100 g and 500 g weights. The 100 g mass was dropped on cartilage-on-bone and cartilage-on-substrate samples while both 100 and 500 g were used for cartilage-only samples. For cartilage only samples, drop heights of 25, 50, 80, and 100 mm were used for the 100 g impact mass and 25, and 50 mm for the 500 g impact mass. Cartilage-on-bone and cartilage-on-substrate used only 100 g impact mass and a drop height of 50 mm. For the substrates, brass (E = 100 GPa), Nylon (E = 3.1 GPa), and cork (E = 0.0035 GPa) were used to provide a wide range of substrate moduli. Energy of impact was calculated using the mass and drop height of the test. Energy of deformation was calculated using the area underneath the loading and unloading curves. The results showed an increase for maximum dynamic modulus, maximum Cauchy stress, and maximum engineering strain for both 100 g and 500 g isolated cartilage impact tests. Mean Cauchy stress rate also increased for both the impact weights but strain rate remained relatively constant. For cartilage-on-bone and cartilage-on-substrate samples, the dynamic modulus of both combinations increased with increasing substrate/bone length until a steady state was reached. Dynamic modulus was higher compared to quasistatic modulus. Overall, the modulus increased rapidly with strain rate.

Edelstein et al. (2010) conducted impact testing of cartilage to measure Poissons ratio of the tissue undergoing large strain at high stress rates. For this study, two experiments were conducted: high-speed video recording to measure the tissue deformation under impact loading of human femoral cartilage plugs, and impact testing of bovine medial metacarpal cartilage plugs to measure the energetic coefficient of restitution. For the video recording experiment, femoral heads of two patients, both 85 years of age and one male and one female, were used for sample extraction. Nine, full-depth samples with a diameter of 5 mm were used. For the impact testing, 83 samples with a diameter of 5mm from a young bovine specimen were extracted. A drop tower equipped with 100 g and 500 g weights was used to apply the impact on the bovine and human samples, respectively. The drop heights

used were 25 mm, 50 mm, 80 mm, and 100 mm for the bovine samples while 25 mm, 50 mm, and 75 mm were used for the human cartilage samples. A Photo-Sonics Phantom V7 high speed video system with a frame rate of 10,600 frames per second was used to record the deformation of the human samples. To calculate the Poissons ratio of the human samples, longitudinal strain, z, and radial strain, r, were recorded. Poissons ratio is then given by:

$$\nu = -\epsilon_r/\epsilon_z$$

For each bovine sample, a loading and unloading curve was produced and used to calculate the energetic coefficient of restitution. The square of the energetic coefficient of restitution is given by:

$${e_*}^2 = -W_r/W_c$$

Where Wr is the energy released during restitution and Wc is the energy of deformation. The results showed that for the human samples, Poissons ratio increased with applied compressive strain. The data collected from the bovine samples suggested that the coefficient of restitution decreased with increasing impact velocity. This is contrary to the idea that cartilage acts more elastically as stress and strain rates are increased. Overall, the researchers were able to characterize the viscoelastic properties of articular cartilage. The study would have further benefited from Poissons ratio calculations for bovine samples and coefficient of restitution calculations for human samples. This would allow for an inter-species comparison Furthermore, the effect of the impacts was not explored. In other studies, 500 g mass dropped from a height of 50 mm caused extensive damage to the cartilage.(6) This could affect the viscoelastic properties measured for that sample.

Thambyah et al. (2010) studied the specifics regarding where in the cartilage matrix the most damage occurs as a result of impact load and how micro-level changes within the matrix affect the response of the tissue as a whole. For this study, 24 bovine patellae

were used for impact testing. 14 x 14 mm samples were cut from the distal-lateral quadrant of each patella with about 6 mm of subchondral bone attached. Each of the samples was classified into three categories: intact-immature, intact-mature, and mildly degenerate. This classification was done by comparing age and the result of an Indian ink stain. No staining suggested intact cartilage and age was the only factor in determining maturity of tissue. The samples were impacted using special impact loading device, which utilized a 1.6 kg rigid pendulum and released at heights ranging from 75 mm to 200 mm. Preliminary results showed an impact energy of about 2.3 J was needed to cause macroscopically visible damage while the slightly degenerated tissue required about 1.6 J, therefore these impact energies were used to determine peak Cauchy stress. Following the test, the tissues were submerged in 10% formalin, washed, and then decalcified with 8% formic acid to decalcify the bone for sectioning. After sectioning, the samples were then placed in 0.15 M saline for examination using differential interference contrast optical microscopy (DIC). For the intact-immature sample group, a peak Cauchy stress of 59.0 8.1 MPa was found and fracture propagation was found to progress radially downward through the tissue. For the intact-mature group a peak Cauchy stress of 65.2 6.6 MPa was found. Failure of the tissue was characterized by small rupture lines on the surface which propagated in the radial direction. Finally, for the mildly degenerate group, a peak Cauchy stress of 44.9 4.4 MPa was found. The tissue showed severe damage through the tissue where entire sections became detached. For all of the previous groups, the force-time curve showed only one distinct peak, while for this group several peaks were shown. Multiple peaks was indicative of failure of the cartilage at multiple layers as opposed to only the top layer being damage for the intact sample groups. The researchers were able to take very fine images of the cartilage post-impact and relate them to the impact testing parameters; however they could have improved on selecting which impact energy to use for the test. The researchers limited their search to only seeing which energy caused macroscopic damage to the tissue.

Energies less than what was selected may also have alter the tissue in a microscopic fashion which could affect the peak stress. This would also be in line with their original question of seeing how micro level structures in the tissue affect the entire impact load response.

Kim et al. (2012) studied the effects of prior creep deformation on the mechanical response to impact loading. For this study, patellae free from any visible defects was collected from two year old bovine bulls and stored in -20oC. Before testing, the samples were thawed and cut into 14 x 14 mm samples. In total, 160 samples were collected and divided into eight different groups. A pendulum attached to a pulley system applied varying amounts of creep loading to prepare the samples for impact testing. The samples were statically compressed with 4 MPa for 0 min, 0.2 min, 1 min, 5 min, 15 min, 30 min, 60 min, and 180 min. Creep displacements were recording using a linear variable differential transformer and force was recorded using a force transducer. For impact loading, the impact energy used was 2.2 J, which came from an indenter pendulum release height of 80 mm; this translates to a mean impact velocity of 1.13 m/s. The equation used to define the impact energy is:

$$E_k = \frac{1}{2} I (\frac{v}{r})^2$$

Where Ek is impact energy, I is the second moment of mass, v is linear velocity of indenter at impact, and r is the radius of the pendulum arm. The properties that were related to creep strain were Impact strain, peak force, impact duration, time to peak force, impulse, and energy lost. A high speed video camera was used to record the progression the impact. Finally, the samples were placed in a flatbed scanner to create high resolution images of the samples for microscopic assessment of damage. Scores were created by the researchers to grade the impact damage. The results showed a high correlation between creep loading and impact tissue response. Increasing creep strain led to a decrease impact strain, raised the mean peak force, and decreased duration of impact and time to reach peak force. No cor-

relation was found with creep strain and impulse or energy loss. No significant differences were found for creep times of 60 to 180 min. For the assessment of structural damage, the researchers stained the samples with India ink and found that most of their samples suffered small fissures and no delamination of the tissue. A few samples showed a range from multiple fissures crossing to complete delamination or severe loss of tissue. The damage did correlate with the amount of creep applied to the samples. Overall, it was found that creep strain does correlate with impact loading behavior of the tissue as well as the damage progression during impact. The scoring system could have been improved, however if instead the researchers used clinically accepted cartilage assessment scores, the presented data would be more relevant to clinicians and other researchers that seek to standardize the damage model of osteoarthritis.

Malekipour et al. (2013) studied the mechanical properties of equine articular cartilage attached to the subchondral bone under impact loading. The properties investigated were strain, peak Youngs modulus, and energy absorption and dissipation. Impact loading was conducted on 13 osteochondral explants of size 9 mm-diameter from one adult racehorse. The explants were fixed in dental cement indented using a 20 mm-diameter indenter and a cyclic half-sine wave compression loading was applied until a strain of 20% was reached and repeated at a frequency of 10 Hz. The compressive force was measured using a 10kN load cell and the strain was measured using a 1000 fps high speed camera that recorded the trajectory of the cartilage-bone interface. Finally, micro CT scanning was done before and after the impact was applied. The results showed much higher energy dissipation within the subchondral bone that has micro-fractures present. It was also observed that articular cartilage behaved similar to an elastic material during impact loading for intact specimens. This behavior was seen with a relatively low energy loss (27.5 23.0%) while a higher energy loss was observed in damaged (cartilage fissures) cartilage specimens (72.3 29.0%). Overall, the researchers were able to find that visible damage to articular carti-

lage and the underlying subchondral bone does affect its compressive strength. However, there is no characterization of the different cartilage fissures present on the samples. The groups being compared are simply ones without fissures and/or bone fractures and ones with those defects present. A relationship between fissure geometry and placement, bone fracture morphology and compressive strength should be explored to further characterize the damaging effects of cartilage and bone defects. The use of Youngs modulus in the study is also a misrepresentation of the tissue response to compression. Using a linear measure for nonlinear behavior is an oversimplification of the tissue response. Although, many studies have researched the effects of impact loading of cartilage, there hasnt been a focus on a detailed analysis of the altered structure of the tissue. Burgin et al. (2014) studied the properties of elderly human articular cartilage by subjecting them to impact and comparing the values to previously collected data with slow loading conditions. 14 human (eight male, six female) full-depth femoral head cartilage samples were subjected to slow, unconfined compression followed by an impacts with 78.5 mJ and 1.25 m/s. The modulus and coefficient of restitution was calculated using the slope of the loading curve and the area underneath the loading and unloading curves, respectively. The tissue composition was then assessed using a variety chemical processes and assays. The results showed little in terms of a relationship between the mechanical properties and the structural changes to the tissue. Change in water retention was undetectable, composition values did not have strong correlation with the modulus; the collagen and water composition together accounted for 25% of the variance found for the modulus. Improvements can be made to the compositional analysis of the cartilage; no analysis was done on the condition of the tissue before and after impact. By doing this, the morphology of the cartilage can be described and related to the mechanical properties. Alterations in the fiber structure will not affect collagen volume fractions but absolutely will affect the compressive strength of the tissue. The current literature provides a very comprehensive picture on the behavior of articular

cartilage. Many different parameters were measured and many variables altered and explored to explain the alterations in structure and function for impact-traumatized cartilage. However, much of the data is subjective and described in a qualitative manner. This leaves much of the data up for various angles of interpretation and the next step to create data worth acting upon is using a standardized means of damage assessment. Cartilage damage markers such as delamination, fissuring, or chondrocyte death must be measured in a way that is accepted by researchers and clinicians alike to be able to create reproducible evidences. This will allow for a more precise understanding of the damage progression that occurs with osteoarthritis.

Chondrocytes, the only cells in healthy cartilage, produce and maintain matrix of enmeshed collagens and proteoglycans in response to the evolving chemical and mechanical environment. *In-vivo* regeneration of mature articular cartilage is limited due largely to the scarce presence of chondrocytes ($<$4% by volume, cf. Mow et al. (2005)). Since cartilage is avascular, the chondrocytes obtain nutrients only through fluid permeation which is enhanced during mechanical loading during joint movement (Archer et al. 1990). Mechanical trauma is dangerous for the health of cartilage and can induce a progressive degeneration of the tissue, e.g. post-traumatic osteoarthritis (OA) (Torzilli et al. 1999).

Such traumas disrupt the microstructure of the extracellular matrix which alters the load-bearing capabilities of tissue. For example, as the network of collagen ruptures or fractures, and enmeshed proteoglycan macromolecules are progressively lost during loading, the tissue's intrinsic permeability reduces. Such a reduction compromises the tissue's ability to retain fluid pressure and applied load progressively shifts from hydrostatic pressure to the solid matrix. This increased loading then aggravates fracturing of the collagen network and the tissue spirals into a cascade of degeneration.

Due to the vulnerability of mature cartilage, previous researchers sought to measure the extent of mechanically-induced permanent damage. To this end many researchers utilized

India Ink staining to visualize macroscale fractures/fissures, cf. Atkinson et al. (1998), Ewers et al. (2001), Kim et al. (2012), Bonnevie et al. (2015), Fischenich et al. (2015). *In vitro* impact trauma is also widely used as analogy for the onset of osteoarthritis, e.g. Duda et al. (2001), Martin et al. (2004), Bush et al. (2005), Bartell et al. (2015). Experiments using impact trauma have also been applied to, e.g.: elucidate cartilage's impact properties, cf. Verteramo and Seedhom (2007), Burgin and Aspden (2008), Burgin et al. (2014); probe cell death after traumatic impact, cf. Ewers et al. (2001), Bush et al. (2005), Natoli et al. (2008); and measure changes within the extracellular matrix, cf. Jeffrey et al. (1995, 1997), Borrelli Jr. et al. (2004). Unfortunately such approaches allow only a macroscopic assessment of gross damage.

Mechanically induced micro-damage of the collagen network, while initially appearing harmless, likely contributes to the accelerated degradation of cartilage. Unfortunately fewer studies have tried to find mechanical thresholds for minute changes to the tissue's ECM. Repo and Finlay (1977) found that impact generating stresses of approximately 25 MPa within the tissue caused structural changes and chondrocyte death. They impacted 43 human specimens using a drop tower; calculated the resulting stress, strain, and energy absorbed; and visualized the resulting damage using scanning electron microscopy (SEM). They reported that stress of 25 MPa (corresponding to strain of 20% – 30%) and impact energy of 1 mJ/mm^3 were sufficient to cause large fractures in the tissue under strain rates of 500 and 1000 (1/s). Atkinson et al. (1998) found that shear stress was the best mechanical predictor for surface fissures in cartilage. They impacted specimens from lateral tibial plateaus of rabbits, recorded the force versus displacement, and verified the presence of fissures using light microscopy. Using finite element analysis they predicted the stresses and strains associated with each impact and applied logistic regression to predict fissures resulting from blunt trauma. Duda et al. (2001) concluded that chondrocyte death preceded visible damage to cartilage tissue. They impacted porcine patellas with energies of 0.06,

0.1, and 0.2 J and looked for damage using staining with India ink and scanning electron microscopy. They found no macroscopically visible structural damage even at 0.2 J.

More recently, Thambyah et al. (2008) concluded that at least two types of failure are possible under impact with an energy of 0.76 J: (i) dramatic disruption of the cartilage surface with microdamage to the underlying bone, and (ii) delamination of the articular surface layer without affecting the bone. They impacted specimens, from the tibial plateau with the meniscus removed, extracted from three males (62-70 years old) human cartilage visualized the results using 3-D reconstructions from SEM and micro-computer tomography (μCT).

In this study we aimed to determine the minimum mechanical insult to cause permanent microstructural damage (micro-fracture) to the network of collagen within human articular cartilage. To this end, we prepared location-matched human cartilage specimens from adult donors and applied a range of low-energy impact loads in unconfined compression, under a range of strain rates. We hypothesized that impact energies well below 0.1 J or 1 mJ/mm^3 would cause microstructural changes to the network of collagen with the ECM. Such changes may initiate the degenerative cascade known as OA.

2 Methods

2.1 Materials and Methods

2.2 Specimen Preparation

Tissue arrived from the Musculoskeletal Transplant Foundation sealed in sterile buffered preservative solution (Penicillin G, Streptomycin sulfate, Polyoxyethylene phenol ether, NCTC Medium 135, Amphotericin B, Fetal calf serum, and DMEM) at 4°C. We harvested human cartilage from the lateral femoral condyles and patellofemoral grooves of six male donors (D1-6, 30.2 $\pm$ 8.82 yrs old, M$\pm$SD). We extracted osteochondral/bone plugs (3 mm diameter) using a circular punch, eighteen specimens per donor for a total of 108 specimens. Using razor and scalpel blades we carefully removed the subchondral bone to create a surface parallel to the articular surface. We ensured that the specimens remained saturation with fluid by spraying specimens with Phosphate Buffered Saline (PBS) during the removal process and storing them in PBS.

Using a digital micrometer (Carrera Precision, resolution 0.01 mm) we measured the thickness of each cartilage specimen, excluding the subchondral bone, and took the average of five measurements. We immersed specimens not immediately tested in PBS and stored them at -80°C, cf. Szarko et al. (2010).

2.3 Low-Energy Impact Testing

We constructed a custom drop tower for these experiments such that we could independently adjust both the total weight and the drop height. Our load carriage included a rack for variable weights and sat within aluminum guide rails which included a height-adjustable release pin. We fitted the load carriage with both an accelerometer ($\pm$49000 m/s^2; 350A14, PCB Piezotronics, Depew, NY) and a force sensor (22.24 kN; 200B05, PCB Piezotronics), mounted in the direction of impact. We connected the accelerometer and force sensor to a signal conditioner (482C16, PCB Piezotronics) using BNC cables and recorded the filtered signal using a data acquisition module (9215, National Instruments, Austin, TX) fitted in a compact data acquisition chassis (cDAQ 9171, National Instruments). We recorded data with a sampling rate of 100,000 Hz.

We mounted specimens on stainless steel platens using cyanoacrylate gel and resubmerged them in PBS solution for >4000 sec prior to imaging in the pristine state. Prior to impact, we brought the specimens up to 37 ± 1°C for >900 sec. Finally, we transferred the platens with mounted specimens from the PBS bath and fitted them into a matching well under the drop tower, and then immediately impacted them while recording the acceleration and force as a function of time. After impact we resubmerged the specimens in PBS solution for >4000 sec prior to imaging in the post-impact state.

We completed the range of tests indicated in Table 2.1 and specimens were assigned to the corresponding test conditions (C1-6), with 18 specimens per condition, resulting in a total of 108 tests.

We completed all of the imaging according to the protocol detailed in Section 2.5.

		Impact Velocity (m/s)	
		0.75	1.0
Impact Energy (J)	0.05	C1	C2
	0.07	C3	C4
	0.09	C5	C6

Table 2.1: Low-energy impact testing: the selected combinations of energies and velocities corresponding to test conditions C1-6.

2.4 Data Analysis

In analyzing the acceleration and force (both versus time) data, we found the beginning of load carriage drop as the point where the acceleration was first approximately $-9.8\,\mathrm{m/s^2}$ and the beginning of impact as the point where the force was first non-zero. Next we determined the peak impact as the maximum value of acceleration and force, which coincided.

We calculated the corresponding velocity and displacement as a function of time by integrating the acceleration data once and twice respectively, following Verteramo and Seedhom (2007). We then calculated the impact velocity and total displacement of the load carriage using data from the beginning of the drop until the beginning of impact. Next, we calculated the total compression of the specimens using data from the beginning of the impact until the peak value of acceleration (and thus force).

We calculated both the engineering strain ϵ $(-)$ and stretch ratio λ $(-)$ applied to specimens as a function of time using

$$\epsilon = \frac{\Delta L}{L_0} \quad \text{and} \quad \lambda = \frac{L}{L_0} = \epsilon + 1, \tag{2.1}$$

where ΔL is the compression of a specimen as a function of time, L is the current height of a specimen as a function of time, and L_0 is the corresponding reference height. Next, we used the force data to calculate both the average first Piola-Kirchhoff (nominal) stress

P (MPa) and Cauchy stress σ (MPa) as a function of time using

$$P = \frac{f}{A_0} \quad \text{and} \quad \sigma = \frac{f\lambda}{A_0}, \tag{2.2}$$

where f is the force applied to the specimens (as a function of time) and A_0 is the corresponding reference cross-sectional area of the specimen.

We calculated the impact energy density input to each specimen E_{imp} (μJ/mm^3) using

$$E_{\text{imp}} = \frac{m v_{\text{imp}}^2}{2V}, \tag{2.3}$$

where m is the mass of the load carriage, v_{imp} is the velocity of the load carriage at the moment of impact, and V is the measured volume of the specimen. Finally, we calculated the energy dissipation density E_{dis} (μJ/mm^3) of the specimens during impact (loading plus unloading) by integrating the stress with respect to engineering strain using

$$E_{\text{dis}} = \int_{\text{loading}} P\lambda \mathrm{d}\epsilon - \int_{\text{unloading}} P\lambda \mathrm{d}\epsilon = \int_{\text{loading}} \sigma \mathrm{d}\epsilon - \int_{\text{unloading}} \sigma \mathrm{d}\epsilon. \tag{2.4}$$

We performed all calculations using MATLAB (The MathWorks Inc., Natick, MA), specifically the built-in function *cumtrapz* was used for all numerical integrations.

2.5 SHG Imaging

Using confocal (multi-photon) microscopy (Carl Zeiss LSM 510, Oberkochen, DE) we imaged the corresponding microstructures of the specimens, specifically the network of collagen. We imaged our specimens using a tunable Ti: Sapphire laser (Coherent Chameleon, Santa Clara, CA) at 850 nm for excitation of the nonlinear signal. We acquired the signals in nondescanned detection using a 425 ± 13 nm band pass filter (FF01-425/26-25; Sem-

rock, Rochester, NY) in front of the detector for the SHG channel. For all sections we used a 20×, 1.0 NA water-immersion objective (W Plan-Apochromat 20×/1.0).

Using a $600 \times 600\,\mu$m (using 2048×2048 pixels) field-of-view in the center of the specimen's articular surface we imaged at increments (step sizes) of 5 μm from the surface down to a depth of $50\,\mu$m. We took both pre- and post-impact images from the center of each specimen. We also marked the orientation of each specimen to keep the pre- and post-impact images consistent.

2.6 Image Analysis

Using the SHG images we looked for the fractures in the network collagen of collagen. We quantified both the width and depth of penetration for each fracture again using MATLAB.

First, using image analysis tools in MATLAB we selected and cropped sections of images that contained fractures. Next we applied a median filter and converted the image to a binary representation. Therein collagen was white while all voids and fractures were black. Using the built-in function *bwdist* we converted the binary images to a distance maps. This function measures the minimum Euclidean distance between a given zero (black) and all non-zero (white) points and reports the pixel distance. Finally, we converted the pixel distance into physical distance and reported the maximum widths of all the fractures in a given specimen after impact. We also calculated the maximum depth of the fractures using the known depth of the fractures from the z-stack.

2.7 Statistical Analysis

First we checked if our results were normally distributed using a Shapiro-Wilk test. If data were normally distribution we reported the mean and standard deviation (M±SD) of

calculated test parameters, or otherwise we reported the median and interquartile range. Next, we correlated both width and depth of fractures in the network of collagen to all test parameters and checked for significance.

To determine the significance of test conditions on microstructural outcomes, we conducted a repeated measures ANOVA. We conducted a logistical regression to correlate predictors (test parameters) impact energy, energy dissipation, nominal stress, nominal stress rate, strain, and strain rate to fracture in the collagen network and then we tested for significance. To avoid the co-dependence of the test parameters we tested each independently. In cases where test conditions significantly correlated with microstructural outcomes we fitted a binary logistic regression plot with a 95% confidence interval.

Thereafter we used an ANOVA test to check for significant differences among patients. Finally, we checked for correlations among test parameters and specimen height.

We completed all statistical analyses using SAS 9.4 (SAS Institute Inc., Cary, NC) with a significance level of 0.05.

3 Results

We completed a total of 108 low-energy impact tests using healthy cartilage specimens from six male donors. Both before and after impact we acquired ten images from each specimen (imaging at the center of, and parallel to, the specimen's articular surface from the surface down to a depth of 50 μm with a step size of 5 μm), resulting in 2160 SHG images for analysis.

The calculated test parameters impact energy density, energy dissipation density, nominal stress, nominal stress rate, strain, and strain rate were normally distributed. None of the specimens showed damage visible to the naked eye following impact and all required confocal microscopy to verify the presence of microstructural damage (if present).

3.1 Low-Energy Impact Testing and Data Analysis

All of the tests showed the same general trends during the impact of the tissue, regardless of impact energy. Figure 3.1 illustrates, using Donor 1, representative data: (a) measured acceleration and force, (b) calculated velocity, and (c) calculated displacement, all versus time.

The measured acceleration data showed a consistent drop at approximately $-9.8\,\mathrm{m/s^2}$ until impact with the specimen. At impact the force data changes from zero to positive. The duration of the impact lasted $\sim$15 ms and was consistent for all specimens.

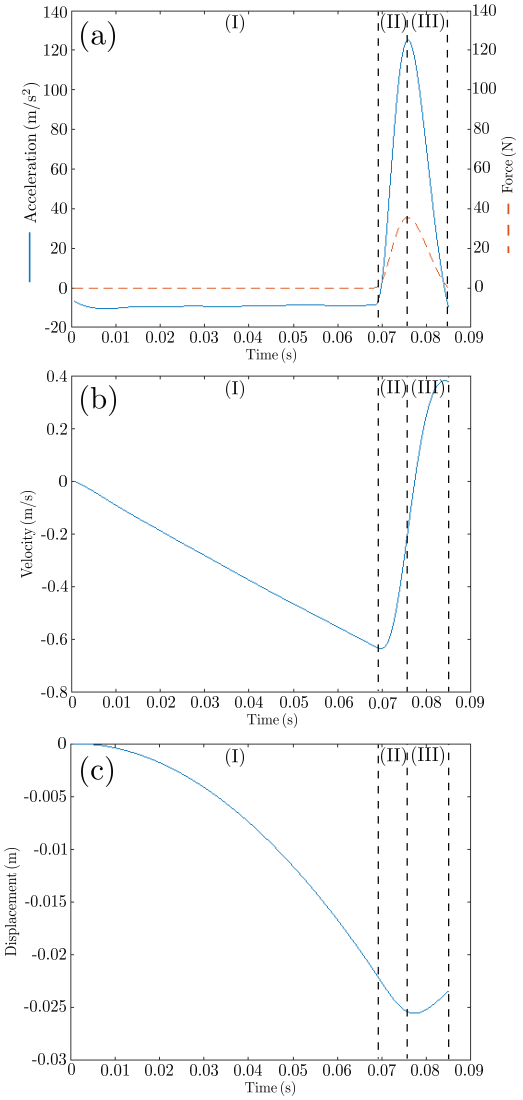

Figure 3.1: Representative test data from Donor 1 versus time: (a) measured acceleration (solid blue) and force (dashed red), (b) calculated velocity, and (c) calculated displacement.

Figure 3.2 illustrates the means and standard deviations for test parameters (predictors). Therein Figs. 3.2(a)–(f) correspond to impact energy density, energy dissipation density, nominal stress, nominal stress rate, strain and strain rate respectively.

We provide the corresponding quantitative data in Appendix A.

3.2 SHG Imaging and Image Analysis

Figure 3.3 illustrates representative SHG images from impacted specimens and the corresponding image analyses of micro-fractures: (a),(b) original SHG images from two-photon microscopy, (c),(d) processed binary images, and (e),(f) resulting distance maps. Both sets of images are from the superficial zone, imaged parallel to the articulating surface and within a depth of $50\,\mu$m.

[Should there be more information about the images? Donor, test condition, etc? Should the images themselves be modified?]

Figure 3.4 illustrates the outcomes for all 108 cartilage specimens impacted in this study, where we show microstructurally fractured specimens (defined as any presence of micro-fractures within the network of collagen) in dark red/blue and undamaged specimens in light red/blue.

3.3 Statistical Analysis

All test parameters used for regression analysis were normally distributed. We correlated both width and depth of fractures in the network of collagen to all test parameters and found no significance. Thus, we correlated our test parameters only with the presence (binary: yes or no) of the fracture in the network of collagen. We found strong correlations between impact energy, energy dissipation, stress and stress rate (independently) and the presence

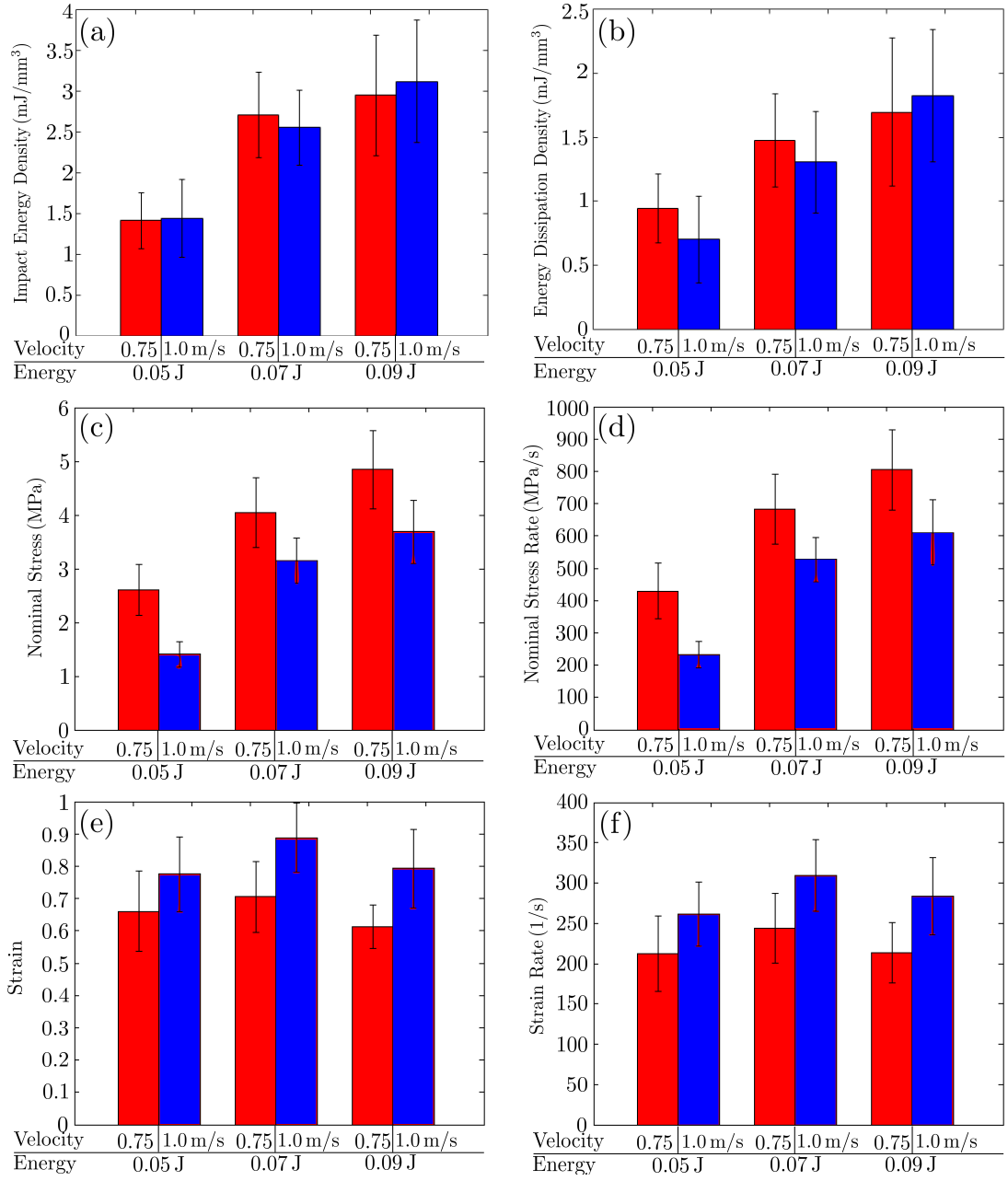

Figure 3.2: Mean and standard deviations (error bars) for predictors (mechanical test parameters): (a) impact energy density, (b) energy dissipation density, (c) nominal stress, (d) nominal stress rate, (e) strain, and (f) strain rate for the six test conditions (C1-6).

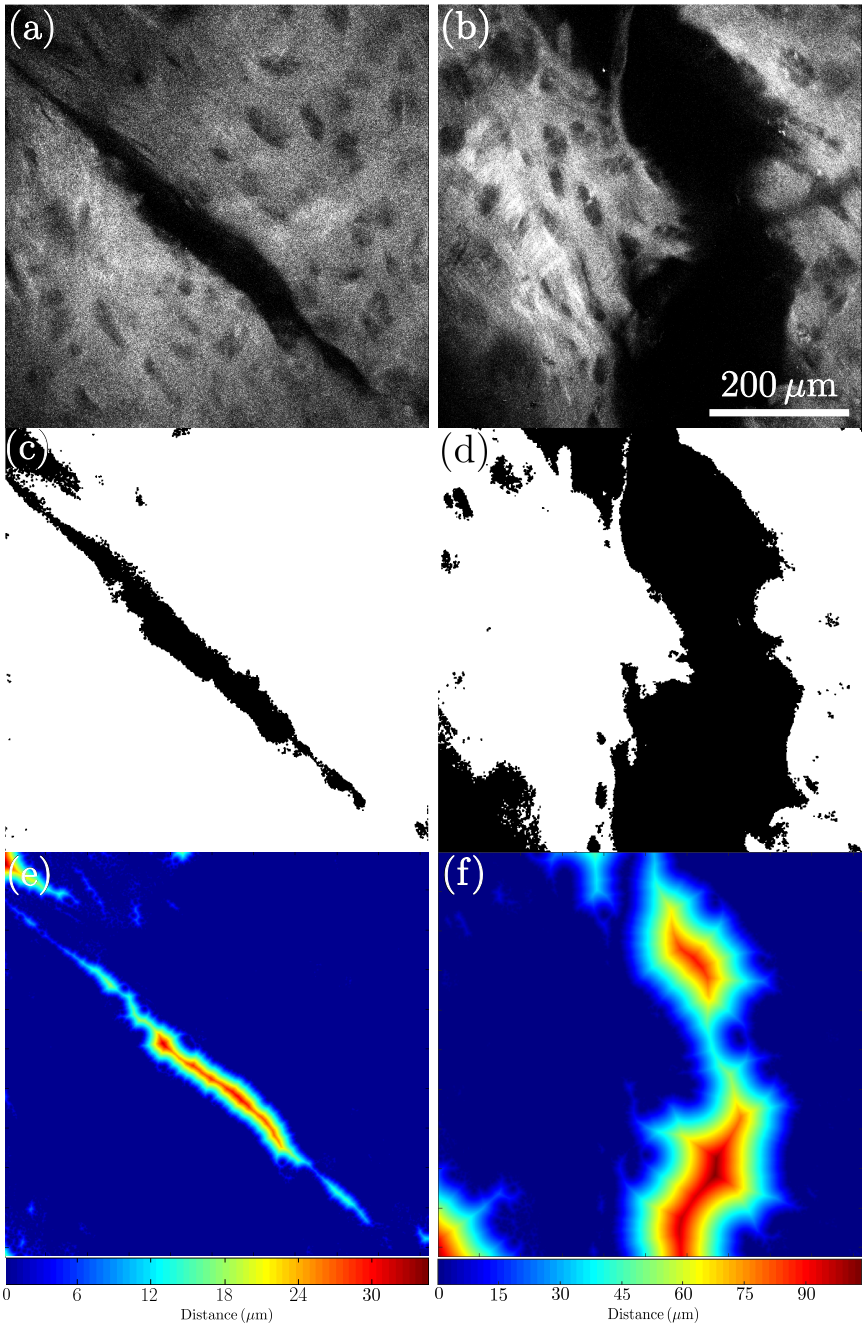

Figure 3.3: Representative second harmonic generation (SHG) images for impacted specimens and the corresponding image analyses of micro-fractures: (a),(b) original SHG images from two-photon microscope (micro-fractures are black), (c),(d) processed binary images (micro-fractures are again black), and (e),(f) resulting quantitative maps of the dimensions of micro-fractures.

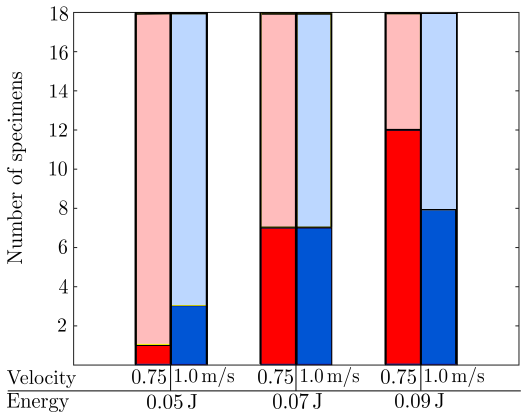

Figure 3.4: Outcomes for all 108 cartilage specimens impacted under the six test conditions (C1-6): microstructurally fractured specimens (any presence of micro-fractures within the network of collagen) in dark red/blue and undamaged specimens in light red/blue.

of microstructural fracture. Interestingly we found no correlation between strain and strain rate (independently) and the presence of fracture. Table 3.1 gives the significance of test parameters, i.e. impact energy density, energy dissipation density, nominal stress, nominal stress rate, strain, strain rate, in predicting microstructural fracture.

Predictor (Test Parameter)	$p-$value
Impact Energy Density	0.0048^*
Energy Dissipation Density	0.0031^*
Nominal Stress	0.0058^*
Nominal Stress Rate	0.0052^*
Strain	0.4684
Strain Rate	0.4288

Table 3.1: Predictors (mechanical test parameters) used for binary logistic regression and the associated p-values where * denotes significance ($p < 0.05$).

Figure 3.5 illustrates the corresponding binary logistic regressions for (a) impact energy density, (b) energy dissipation density, (c) nominal stress, and (d) nominal stress rate.

There was no significant difference found between patients for all test parameters. Furthermore, there were no significant correlations among test parameters and specimen height.

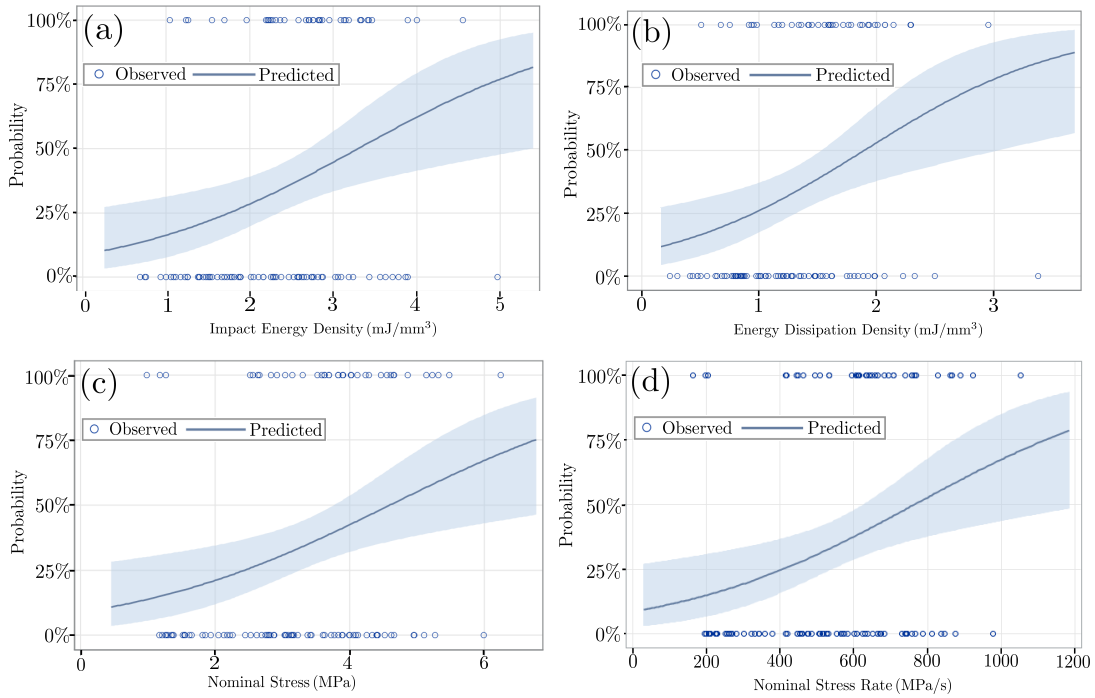

Figure 3.5: Predicting the probability of microstructural fracture in the network of collagen: binary logistic regression plots for (a) impact energy density, (b) energy dissipation density, (c) nominal stress, and (d) nominal stress rate.

4 Discussion

We aimed to determine the minimum mechanical trauma needed to cause permanent microstructural changes to the ECM of human articular cartilage. Our results support the hypothesis, e.g. an impact energy density as low as 0.208 mJ/mm^3 corresponded to a 10% probability of micro-fractures in the network of collagen within human cartilage, and the probability of micro-fractures increased with increasing impact energy densities. We also found that impact energy density, energy dissipation density, nominal stress, and nominal stress rate were significant mechanical predictors of micro-fractures to the network of collagen induced by blunt impact trauma while both strain and strain rate were not.

4.1 Low-Energy Impact Testing and Data Analysis

Figure 3.1 shows a total impact time of $\sim$15 ms, which falls within the range of impact times previously reported (Verteramo and Seedhom 2007, Thambyah and Broom 2010). Trends in acceleration, velocity and displacement are also consistent with those reported previously. Figure 3.2 (also summarized quantitatively in Table **??**) shows the mechanical result of input test conditions C1-6 in terms of impact energy density, energy dissipation density, nominal stress, nominal stress rate, strain, and strain rate. For all three input energies, the higher impact velocity resulted in lower impact energy densities, lower energy dissipation densities, lower nominal stresses, higher nominal stress rates, higher peak engi-

neering strains, and peak strain rates. Overall, the stresses reported in this study are lower than previously reported, due to the lower input energies selected for this study, while the strains are on the order of those reported previously, e.g. Verteramo and Seedhom (2007), Burgin et al. (2014).

[Include a discussion on the influence or likely influence of strain rate on the probability of micro-fractures? Strain rates reported here are lower than those reported in the literature, potentially making our results conservative from this perspective.]

Using results from preliminary studies we selected the desired range of impact velocities and energies. Given the desired impact velocity we used $h = v_{\text{imp}}^2/(2g)$ to determine the required drop height h, where g the gravitational acceleration. Finally, given the desired impact energy we used $m = E_{\text{imp}}/(gh)$ to determine the required mass of the load carriage.

4.2 SHG Imaging and Image Analysis

Figures 3.3(a),(b) show SHG images similar to those previously reported, e.g. Brockbank et al. (2008) and Novakofski et al. (2014). The SHG images shows fracture occurring in the center of the specimen, chosen to be furthest from the cutting effects found at the edges. In preliminary studies micro-fractures appeared to initiate at the articular surface, thus we deemed imaging to a depth of 50 μm sufficient to identify the characteristics of fractures. Furthermore, the micro-fractures seemed to rarely extend beyond 50 μm, similar to previous studies (Repo and Finlay 1977, Atkinson et al. 1998).

Figure 3.4 shows the outcomes for all 108 cartilage specimens impacted in this study, where we show microstructurally fractured specimens in dark red/blue and undamaged specimens in light red/blue. Increasing impact energy shows a clear trend with increasing micro-fracture while velocity does not.

We selected SHG as our imaging modality because of its acute sensitivity to the presence

of collagen. Additionally, imaging the SHG has the following benefits: (i) it preserves the *in situ* fluid-saturated conditions of the tissue (similar to *in vivo* conditions), (ii) it requires no special specimen preparation, and (i) it's relatively fast to generate a z-stack of images.

We imaged all cartilage specimens both before and after impact to help separate lacunae from true micro-fractures generated by impacts. Using our custom image analysis software we calculated the maximum width and depth of micro-fractures in the network of collagen within all samples.

4.3 Statistical Analysis

Table 3.1 shows the significance (p-values) of all of our mechanical test parameters as predictors for micro-fracture in the network of collagen. Increasing the specified input energy clearly increases in the frequency of micro-fracture. Impact energy density, energy dissipation density, nominal stress, and nominal stress rate were all significant predictors ($p < 0.05$) while strain and strain rate were not. Thus micro-fracturing of the network of collagen in cartilage specimens is load induced and not deformation induced. Previous studies have shown that stress-based measures have better correlations with damage parameters than deformation-based measures, e.g. Atkinson et al. (1998), Fischenich et al. (2015).

Figure 3.5 shows the corresponding probability plots for the significant predictors impact energy density, energy dissipation density, nominal stress, and nominal stress rate as predictors for micro-fracture in the network of collagen, cf. Atkinson et al. (1998). In our test configuration, an impact energy density of 3.30 mJ/mm^3, an energy dissipation density of 1.90 mJ/mm^3, a nominal stress of 4.60 MPa, and a nominal stress rate 764 MPa/s all corresponded to a 50% probability of micro-fracture in the network of collagen. With these plots it's possible to estimate the probability of micro-fracture in the collagen network due

to mechanical impact. For example, thresholds for a 10% probability of micro-fractures in the collagen network were impact energy densities of 0.208 mJ/mm^3, energy dissipation densities of 0.009 mJ/mm^3, nominal stresses of 2.79 MPa, and nominal stress rates of 51.5 MPa/s.

Fracture width and depth did not correlate with the severity of impact. Perhaps patient-specific variabilities in cartilage tissues may dictate the path of fracture (Atkinson et al. 1998).

4.4 Limitations and Outlook

There are several limitations of this study. Specimens may not of been extracted exactly perpendicular to the cartilage surface, potentially causing non-uniform application of load and SHG images which were not parallel to the articular surface. The small size of the specimens compromises the ability to replicate *in vivo* conditions of articular cartilage, where the neighboring tissue is likely important in supporting and absorbing mechanical trauma. Hence, the effects of impact may not be as dramatic *in vivo* in light of the supporting subchondral bone and surrounding cartilage. We calculated stress and strain only along the axis of impact, ignoring stresses and strains induced by in other axes (i.e. the full multi-axial state of stress/strain). Finally, friction in our impactor resulted in impact energies slightly lower than those intended in Table 2.1. Thus, we correlated micro-fracture with the actual impact energy density calculated based on the true kinetic energy delivered to each specimen.

Our SHG images showed only $\sim$5% of the total specimen area, which may cause false negatives within our results, potentially weakening our measurement of the fracture threshold. The mechanical parameters measured may include fractured material, such that the stresses and strains necessary for micro-fracture may be below the reported values.

Predicting the threshold for fracture of articular cartilage may allow the development of safety guidelines to reduce the likelihood of onset of post-traumatic osteoarthritis. The network of collagen fibers, and its interactions with large complexes of proteoglycan, is the most mechanically important constituent of articular cartilage. Thus, understanding changes to this network due to mechanical impact may lead to a better recommendations to avoid the initiation and long-term effects osteoarthritis.

In addition, better understanding of the performance of articular cartilage with respect to impact loading, may provide improved targets for the development of man-made cartilage substitutes, i.e. tissue engineering.

Finally, the data presented here may help in developing and calibrating computational models of cartilage and joints, e.g. aimed at predicting damage induced to articular cartilage under mechanical trauma. In the future we aim to apply our results to better understand the initiation of cartilage degeneration and to inform computational models of tissue damage or remodeling, e.g. Stender et al. (2015).

Bibliography

Archer, C. W., McDowell, J., Bayliss, M. T., Stephens, M. D., Bentley, G., 1990. Phenotypic modulation in sub-populations of human articular chondrocytes in vitro. J. Cell Sci. 97, 361–371.

Atkinson, T. S., Haut, R. C., Altiero, N. J., 1998. Impact-induced fissuring of articular cartilage: An investigation of failure criteria. J. Biomech. Eng. 120, 181–187.

Bartell, L. R., Fortier, L. A., Bonassar, L. J., Cohen, I., 2015. Measuring microscale strain fields in articular cartilage during rapid impact reveals thresholds for chondrocyte death and a protective role for the superficial layer. J. Biomech. 48, 3440–3446.

Bonnevie, E., Delco, M., Fortier, L., Alexander, P., Tuan, R., Bonnassar, L., 2015. Characterization of tissue response to impact loads delivered using a hand-held instrument for studying articular cartilage injury. Cartilage 6, 226–232.

Borrelli Jr., J., Zhu, Y., Burns, M., Sandell, L., Silva, M. J., 2004. Cartilage tolerates single impact loads of as much as half the joint fracture threshold. Clin. Orthop. Relat. Res. 426, 266–273.

Brockbank, K. G. M., MacLellan, W. R., Xie, J., Hamm-Alvarez, S. F., Chen, Z. Z., Schenke-Layland, K., 2008. Quantitative second harmonic generation imaging of cartilage damage. Cell and Tissue Banking 9, 299–307.

Burgin, L. V., Aspden, R. M., 2008. Impact testing to determine the mechanical properties of articular cartilage in isolation and on bone. J. Mater. Sci. Mater. Med. 19, 703–711.

Burgin, L. V., Edelsten, L., Aspden, R. M., 2014. The mechanical and material properties of elderly human articular cartilage subject to impact and slow loading. Med. Eng. Phys. 36, 226–232.

Bush, P. G., Hodkinson, P. D., Hamilton, G. L., Hall, A. C., 2005. Viability and volume of in situ bovine articular chondrocytes changes following a single impact and effects of medium osmolarity. Osteoarthritis Cartilage 13, 54–65.

Duda, G. N., Eilers, M., Loh, L., Hoffman, J. E., Kääb, M., Schaser, K., 2001. Chondrocyte death precedes structural damage in blunt impact trauma. Clin. Orthop. Relat. Res. 393, 302–309.

Ewers, B. J., Dvoracek-Driksna, D., Orth, M. W., Haut, R. C., 2001. The extent of matrix damage and chondrocyte death in mechanically traumatized articular cartilage explants depends on rate of loading. J. Orthop. Res. 19, 779–784.

Fischenich, K. M., Button, K. D., Coatney, G. A., Fajardo, R. S., Leikert, K. M., Haut, R. C., Donahue, T. H., 2015. Chronic changes in the articular cartilage and meniscus following traumatic impact to the lapine knee. J. Biomech. 48, 246–253.

Jeffrey, J. E., Gregory, D. W., Aspden, R. M., 1995. Matrix damage and chondrocyte viability following a single impact load on articular cartilage. Arch. Biochem. Biophys. 322, 87–96.

Jeffrey, J. E., Thomson, L. A., Aspden, R. M., 1997. Matrix loss and synthesis following a single impact load on articular cartilage in vitro. Biochim. Biophys. Acta 1334, 223–232.

Kim, W., Thambyah, A., Broom, N., 2012. Does prior sustained compression make cartilage-on-bone more vulnerable to trauma? Clin. Biomech. 27, 637–645.

Martin, J. A., Brown, T., Heiner, A., Buckwalter, J. A., 2004. Post-traumatic osteoarthritis: The role of accelerated chondrocyte senescence. Biorheology 41, 479–491.

Mow, V. C., Gu, W. Y., Chen, F. H., 2005. Structure and function of articular cartilage and meniscus. In: Mow, V. C., Huiskes, R. (Eds.), Basic Orthopaedic Biomechanics & Mechano-Biology. Lippincott Williams & Wilkins, Philadelphia, pp. 181–258, 3rd edition.

Natoli, R. M., Scott, C. C., Athanasiou, K. A., 2008. Temporal effects of impact on articular cartilage cell death, gene expression, matrix biochemistry, and biomechanics. Ann. Biomed. Eng. 36, 780–792.

Novakofski, K. D., Williams, R. M., Fortier, L. A., Mohammed, H. O., Zipfel, W. R., Bonassar, L. J., 2014. Identification of cartilage injury using quantitative multiphoton microscopy. Osteoarthritis Cartilage 22, 355–362.

Repo, R. U., Finlay, J. B., 1977. Survival of articular cartilage after controlled impact. J. Bone Joint Surg. 59, 1–2.

Stender, M. E., Regueiro, R. A., Klisch, S. M., Ferguson, V. L., 2015. An equilibrium constitutive model of anisotropic cartilage damage to elucidate mechanisms of damage initiation and progression. J. Biomech. Eng. 137, 081010.

Szarko, M., Muldrew, K., Bertram, J. E. A., 2010. Freeze-thaw treatment effects on the dynamic mechanical properties of articular cartilage. BMC Musculoskeletal Disorders 11, 1–8.

Thambyah, A., Broom, N., 2010. How subtle structural changes associated with maturity and mild degeneration influence the impact-induced failure modes of cartilage-on-bone. Clin. Biomech. 25, 737–744.

Thambyah, A., Shim, V. P. W., Chong, L. M., Lee, V. S., 2008. Impact-induced osteochondral fracture in the tibial plateau. J. Biomech. 41, 1236–1242.

Torzilli, P. A., Grigiene, R., Jr., J. B., Helfet, D. L., 1999. Effect of impact load on articular cartilage: cell metabolism and viability, and matrix water content. J. Biomech. 121, 433–441.

Verteramo, A., Seedhom, B. B., 2007. Effect of a single impact loading on the structure and mechanical properties of articular cartilage. J. Biomech. 40, 3580–3589.